

GPS bla bla bla

by

Qian Yang

A dissertation submitted in partial fulfillment
of the requirements for the degree of
Doctor of Philosophy
School of Geosciences
College of Arts and Sciences
University of South Florida

Major Professor: Timothy H. Dixon, Ph.D.
Rocco Malservisi, Ph.D.
Don Chambers, Ph.D.
Ping Wang, Ph.D.

Date of Approval:
March X, 2016

Keywords: high precision GPS, ground deformation, Greenland ice mass loss, ice-ocean interactions, carbon-sequestration

Copyright © 2015, Qian Yang

Table of Contents

List of Tables	ii
List of Figures	iii
Abstract	vi
1 InSAR Monitoring of Ground Deformation Due to CO ₂ injection at an Enhanced Oil Recovery Site, West Texas	1
1.1 Abstract	1
1.2 Introduction	1
1.3 Study area description	3
1.4 Observed ground deformation	4
1.5 Simulation	5
1.5.1 Analytical solution for ground displacement	5
1.5.2 Input parameters of the analytical simulations	8
1.5.3 Injection and production data during 2004 - 2011	9
1.6 Simulation results	10
1.7 Discussion	12
1.8 Conclusions	13
1.9 Acknowledgements	14
1.10 References	15

List of Tables

Table 1.1	Reservoir homogeneous properties used for pressure change calculation.	19
Table 1.2	Fluid properties at depth (16MPa,41.5 °C).	20
Table 1.3	Highest pressure buildup and best-fit Young's modulus at three levels of porosity and permeability.	21

List of Figures

Figure 1.1	a) Total LOS (line of sight) displacement from January 08, 2007 to March 06, 2011. b) A SAR intensity image of the study area. Red star represents location of the town of Snyder, Texas. Light grey lines are county boundaries and county names are labeled. Red lines are the boundaries of our study area, Scurry County. Blue line is the approximate boundary of the oil field in the study area. Black dashed line represents location of a profile for surface displacement modeling in the following sections.	23
Figure 1.2	Injection and production history of the study site. Phase I is the primary recovery phase. Phase II is the secondary recovery phase. Phase III is the tertiary/enhanced oil recovery phases. Volumes of fluid injection and production are reported at 16 MPa, 41.5 °C (pressure and temperature at reservoir depth). HC is hydrocarbon.	24
Figure 1.3	DEM of our study area. Black lines are the boundaries of the area covered by the interferogram. Red star represents location of the town Snyder, Texas.	25
Figure 1.4	a) Comparison between Line of Sight (LOS) displacement at Snyder (red star marked in Figure 1) and cumulative volumes of stored (injection minus production) CO ₂ and water in the field from January 2007 to March 2011. b) The total volumes of injected/produced/stored CO ₂ , water, oil and HC gas in the field from January 2007 – March 2011. Volumes of fluid injection and production are reported at 16 MPa, 41.5 °C.	26
Figure 1.5	Map of study area, showing total LOS displacement from January 08, 2007 to March 06, 2011, a) wells injecting CO ₂ (green circle) and water (blue circle), and b) well producing CO ₂ , water, Oil and HC gas (red triangle).	27
Figure 1.6	Location of virtual wells for each type fluid and the average monthly injection/production rate for each virtual well. Circles represent injection wells and triangles represent production wells. Volumes of fluid injection and production are reported at 16 MPa, 41.5 °C.	28

Figure 1.7	Calculated pressure change due to fluid injection and production at three levels of porosity and permeability. (a-c: low porosity/permeability; d-f: medium porosity/permeability; g-i: high porosity and permeability). a,d and g are calculated pressure buildup due to net CO ₂ injection. b, e and h are derived from net water injection. c, f and I are derived from oil and HC gas production	29
Figure 1.8	Calculated pressure change due to all injection and production activities at three levels of porosity and permeability. a) low porosity/permeability level; b) medium porosity/permeability level; c) high porosity and permeability level.	30
Figure 1.9	Goodness of fit versus Young's modulus at three levels of pressure change conditions. Simulated LOS displacements are fitted to LOS displacement observation along the profile shown in Figure 1. Note that the minimum value of Young's modulus is well constrained, but the upper bound value is not.	31
Figure 1.10	Simulated LOS displacement at three levels of pressure change conditions versus InSAR observation along the profile shown in Figure 1.	32
Figure 1.11	Comparison between simulated LOS displacements and InSAR observation for the entire study area. Surface displacements were derived from high-pressure change condition. a) Simulated LOS displacements; b) InSAR observation; c) residual.	33

Abstract

hjhkhjkajdl jd jljkjh kjl

1. InSAR Monitoring of Ground Deformation Due to CO₂ injection at an Enhanced Oil Recovery Site, West Texas ¹

1.1 Abstract

Interferometric Synthetic Aperture Radar (InSAR) measurements have been used to measure ground deformation associated with fluid injection/production at an Enhanced Oil Recovery (EOR) field in Scurry County, West Texas. 100 million tons (Mt) of supercritical CO₂ have been sequestered here since 1972, of which about half has been sequestered since 2004. InSAR data show surface uplift up to 10 cm in the field between January 2007 and March 2011. We evaluated data concerning injection and production of CO₂, water, oil and hydrocarbon gas from 2004 to 2011 to investigate causes of the observed uplift. An analytical model is used to calculate reservoir pressure change and surface displacement. Our simulations show up to 10 MPa pressure buildup in the reservoir over four years of net injection and production. Surface displacement predictions agree well with the InSAR observations. Water injection alone cannot explain the 2007 – 2011 surface uplift because the net injected water (\sim 1 Mt) is negligible compared to the net injected CO₂ (\sim 24 Mt). The predicted total pressure buildup (up to 10 MPa) consists of net CO₂ injection (up to 12 MPa), net water injection (up to 2 MPa), and oil and gas production (up to -0.4 MPa). Hence, observed ground uplift was mainly caused by CO₂ injection.

1.2 Introduction

An important aspect of large-scale Carbon Capture, Utilization and Storage (CCUS) is the ability to assess the fate of injected CO₂ and test for leakage. These so-called Moni-

¹This chapter has been reprinted from the International Journal of Greenhouse Gas Control with permission as: Yang, Q., Zhao, W. L., Dixon, T. H., Amelung, F., Han, W. S., Li, P., (2015), InSAR Monitoring of Ground Deformation Due to CO₂ injection at an Enhanced Oil Recovery Site, West Texas, International Journal of Greenhouse Gas Control, 41, 20-28.

toring, Verification and Accounting (MVA) activities typically involve active seismic surveys and down-hole techniques for precise tracking of CO₂ plume migration, both of which can be expensive. Since the economic viability of CCUS is impacted by the cost of MVA activities, development of lower cost approaches is desirable.

Injection of CO₂ or other fluid into a reservoir at depth increases fluid pressure in the reservoir, causing deformation in the overlying strata and inducing surface deformation. If the pressure change is large enough, the surface deformation may be measurable. In principle, the measured surface deformation can be inverted to estimate pressure changes at depth and track the CO₂ plume (e.g., Vasco et al., 2008, 2010; Rinaldi and Rutqvist, 2013; White et al., 2014; Karegar et al., 2015). Over long periods (decades or centuries), chemical reactions that result in formation of mineral phases will cause pressure and volume reduction and subsidence, and could not be distinguished from migration or leakage with this technique alone. On the other hand, surface deformation can be measured at relatively low cost, the interpretation is relatively straightforward, and the technique gives useful information in the critical few years immediately following injection.

Enhanced Oil Recovery (EOR) refers to techniques for increasing the amount of oil extracted at depleted or high viscosity oil fields. CO₂-Enhanced Oil Recovery (CO₂-EOR) has been used by the oil and gas industry for over 40 years (Orr and Taber, 1984), but only recently has its potential as a promising method of carbon sequestration been realized and investigated (Bryant et al., 2007). Considering the potential of CO₂-EOR for implementation of large-scale carbon emission reduction (Metz et al., 2005), it is important to test surface deformation MVA techniques in a CO₂-EOR field.

Interferometric Synthetic Aperture Radar (InSAR) technique has been successfully used to monitor surface deformation associated with CO₂ injection at the In Salah field in Algeria (Mathias et al., 2009a; Morris et al., 2011; Shi et al., 2012; Verdon et al., 2013). In this paper, we use InSAR to study surface deformation associated with a CO₂-EOR project in West Texas. We use an analytical model and historical injection and production data to

estimate CO₂ plume extent and reservoir pressure change constrained by surface deformation observations. The study reveals that ground uplift between January 2007 and March 2011 is mainly caused by CO₂ injection. The maximum pressure change due to net injection and production of CO₂, water, oil and hydrocarbon gas is up to 10 MPa.

1.3 Study area description

The CO₂-EOR field is located in Scurry County, West Texas (Figure 1.10). The reservoir is the southeastern segment of the Horseshoe Atoll play within the Midland basin, one of the largest subsurface limestone reef mounds in the world (Galloway et al., 1983). It is a chain of oil fields with the major one being the Kelly-Snyder field. The producing zones are Pennsylvanian-aged Cisco and Canyon formations, and are comparable to a large class of potential brine storage reservoirs. Average depth of the producing zones is 2000 m (Vest Jr, 1970; Raines and Dobitz, 2001) with average reservoir pressures of 16 MPa and a temperature of 41.5 °C (Raines, 2005). The rock formation porosity (0 – 22.5%) and permeability (0.1 md – 1760 md) are described in Raines (2005). The reported average porosity and permeability are 9.8% and 19 mD respectively. Overlying the producing zone is the Permian-aged Wolfcamp formation, providing a very low permeability seal above the Cisco and Canyon Groups. The physical properties of the field make it a good candidate for CO₂-EOR as well as CO₂ sequestration.

Three production phases occurred in the oil field after it was discovered in 1948 (Figure 1.2). The primary recovery phase was 1948 – 1951. During this phase, 5 percent of original oil in place (2.73 billion barrels) was produced by the solution gas driven mechanism, resulting in decline of the original reservoir pressure by 50 percent, from 21.5 MPa to 11.4 MPa (Dicharry et al., 1973; Brummett Jr et al., 1976). The secondary recovery phase began in 1954. During this phase, water-flooding technology was used to produce oil and maintain reservoir pressure. 133 MCM (Million Cubic Meters) of water was injected into the reservoir, and reservoir pressure increased from 11.4 MPa to 16.2 MPa. However, after 17 years of water injection, over 40 percent of original oil in place was still left in the reservoir.

The tertiary/enhanced oil recovery phase started in 1972 (Crameik et al., 1972). During this phase, CO₂ was injected continuously into the reservoir to increase oil production. From 1972 to 2003, the CO₂ monthly injection rate was quite stable, with a mean value of 0.28 MCM per month. The CO₂ injection rate has increased since 2004. The mean value of the CO₂ monthly injection rate in 2004 – 2011 was about six times higher compared to 1972 – 2003. Although water was also injected into the unit during the third phase, the sequestered water was small compared to the sequestered CO₂ since injected and produced volumes of water are approximately equal (Figure 1.2). Raines (2005) suggested that approximately 55 Mt (70 MCM) of CO₂ was sequestered in the reservoir from 1972 to 2005 based on a simple mass-balance model. Our study updates the injection and production data sets to 2011, and suggests that about 100 Mt (128 MCM) of CO₂ were sequestered in the reservoir from 1972 to 2011, with about 50 percent accumulated from 2004 to 2011. Note that in this paper, all the volume numbers are reported at the reservoir depth with pressure equal to 16 MPa and temperature equal to 41.5 °C.

1.4 Observed ground deformation

Advanced Land Observing Satellite (ALOS) image data from the Japan Aerospace Exploration Agency (JAXA) are used to monitor surface displacement above the CO₂-EOR field. The satellite repeat cycle is 46 days. Thirteen images were acquired from January 08, 2007 to March 06, 2011 on ascending path 184, frame 640, from which 53 interferograms were generated. The small Baseline Subset technique (Berardino et al., 2002) is applied to generate displacement time series. By using L-band SAR data, the interferometric phase tends to remain coherent even in vegetated areas. To reduce errors caused by phase unwrapping, we use the temporal coherence method (Pepe and Lanari, 2006) to mask out pixels with unwrapping error. SRTM version 4 (Reuter et al., 2007) 3 arc second DEM data were interpolated to 1 arc second (\sim 30 m) resolution to remove topographic effects (Figure 1.3).

A total displacement of up to \sim 10 cm LOS (line of sight) is detected (Figure 1.10a). Note that part of the oil field is not covered by our interferograms. No active injection

or production occurred in this section during the InSAR observation period (discussed in section 4.3, Figure 5). Thus, we expect only moderate displacement here associated with nearby injection and production activity.

Figure 1.4a shows time series of LOS displacement at Snyder, Texas (red star marked in Figure 1). Increasing LOS displacement is observed from 2007 to 2011 when the cumulative volume of sequestered CO₂ increased. From 2007 to 2011, about 31 MCM (~ 24 Mt) CO₂ is stored in the reservoir, significantly larger than the amount of stored water (\sim MCM/1 Mt) (Figure 1.4b), suggesting that the observed surface uplift is mainly caused by CO₂ injection.

1.5 Simulation

1.5.1 Analytical solution for ground displacement

An analytical solution for ground displacement associated with injection or withdrawal of fluid at depth may be derived in two steps: a) the approximate solution for reservoir pressure change due to fluid injection (Mathias et al., 2009a,b) and production (Theis, 1935); and b) the solution for surface deformation due to pressure change in depth estimated in an elastic half space (Xu et al., 2012).

First, we calculate the reservoir pressure change field due to fluid injection. Here, the approximate solution of Mathias et al. (2009a) is adopted to calculate pressure buildup due to injection of CO₂ in rock formations with large spatial extent. This solution is derived using the method of matched asymptotic expansions and accounts for two-phase Forchheimer flow (supercritical CO₂ and water), allowing for slight compressibility of fluid and rock formation. We also use the solution of Mathias to calculate pressure buildup due to water injection. Note that the Mathias solution reduces to the Theis (1935) solution for calculating pressure change due to water injection (single-phase flow) (Mathias et al., 2009a). We adopt the Theis solution to estimate pressure decline caused by fluid extraction (oil, hydrocarbon gas, water and CO₂). Theis (1935) provides a simplified model to estimate pressure drawdown due to pumping in a homogeneous, isotropic and infinite areal extent reservoir. We apply the Mathias solution to each injection well and calculate pressure change field caused by

CO_2 injection and water injection respectively. Note that for wells injecting both CO_2 and water, we calculate the induced pressure buildup separately regardless of the mixing nature. As with pressure change due to injection, we apply the Theis equation to calculate pressure change field caused by pumping of each type of fluid (oil, hydro-carbon gas, water and CO_2) at every individual production well. In summary, in this step we estimate a pressure change field caused by every single fluid element injected/extracted at an individual well, in preparation for surface displacement calculation in the next step.

Here we summarize the main formulations of the analytical solution for pressure buildup $P_{inj}(r, t)$ at radial distance r (note that x is dependent on r) and time t due to fluid (CO_2 /water) injection (Mathias et al., 2009a) (eq. 1-2) and the Theis solution for pressure drawdown $P_{pro}(r, t)$ due to fluid (CO_2 /water/oil/HC gas) production (eq. 3).

$$P_{inj}(r, t) = P_0 \left\{ \frac{1}{2\gamma} Ei\left(\frac{\alpha x}{4\gamma}\right) + \frac{1}{2\gamma} \left(\ln\left(\frac{\alpha x}{4\gamma}\right) + 0.5772 \right) \right. \\ \left. + P_0 \begin{cases} -\frac{1}{2} \ln\left(\frac{x}{2\gamma}\right) - 1 + \frac{1}{\gamma} - \frac{1}{\gamma} \left(\ln\left(\frac{\alpha x}{2\gamma^2}\right) + 0.5772 \right) & x \leq 2\gamma \\ -\left(\frac{x}{2\gamma}\right)^{0.5} + \frac{1}{\gamma} - \frac{1}{2\gamma} \left(\ln\left(\frac{\alpha x}{2\gamma^2}\right) + 0.5772 \right) & 2\gamma \leq x \leq \frac{2}{\gamma} \\ -\frac{1}{2\gamma} \left(\ln\left(\frac{\alpha x}{4\gamma}\right) + 0.5772 \right) & x \geq \frac{2}{\gamma} \end{cases} \right\} \quad (1.1)$$

where: Ei is the exponential integral operator.

$$P_0 = \frac{Q_m \mu_f}{2\pi H \rho_f \kappa} \\ \gamma = \frac{\mu_f}{\mu_{brine}} \\ x = \frac{(r/r_w)^2}{t Q_m / (2\pi \omega H (r_w)^2 \rho_f)} \\ \alpha = \frac{Q_m \mu_f (c_{rock} + c_{brine})}{2\pi H \kappa} \quad (1.2)$$

where: r is the radial distance to injection well (m); r_w is the injector well radius, and we use $r_w = 0.1 m$ for our calculation; ρ_f is the density of injected fluid (kg/m^3); μ_f is the viscosity

of injected fluid ($Pa \cdot s$); Q_m is the mass injection rate (kg/s); t is the injection time (s); c_{rock} is the formation compressibility (Pa^{-1}); κ is the formation permeability (m^2); μ_{brine} is the brine compressibility (Pa^{-1}); H is the formation thickness (m).

$$P_{pro}(r, t) = -\frac{Q_\nu \mu_f}{4\pi \kappa H} Ei\left(-\frac{\mu_f(\phi c_f + c_{rock})r^2}{4\kappa t}\right) \quad (1.3)$$

where: Q_ν is the volume injection rate (m^3/s); μ_f is the viscosity of produced fluid ($Pa \cdot s$); c_f is the compressibility of produced fluid (Pa^{-1}); ϕ is the formation porosity; other parameters are the same as in eq. 1 and eq. 2. Values of those parameters used in computing the pressure change are listed in Table 1.1 - 1.2.

Second, given the calculated fluid pressure field, we then calculate induced surface displacement. Xu et al. (2012) provide an analytical elastic solution for displacement in a half space forced by an arbitrary pressure distribution in the reservoir. Since the pressure caused by injection/production at individual well can be approximated as radial distribution, we first use Xu's solution to estimate surface displacement centered at each well according to the radial distributed pressure field of that well. Then, surface displacement of each well is linearly summed up to get the total surface displacement field due to all injection and production activities.

The main formulations of the analytical solution for vertical displacement $u_z(r)$ and horizontal displacement $u_r(r)$ at the radial distance r at the free surface results from the cumulative contribution of all the rings of dilation at radius r_0 and depth z' Xu et al. (2012).

$$\begin{aligned} u_z(r) &= -\frac{2(1+\nu)(1-2\nu)}{\pi E} \iiint_{00Z_1}^{\infty\pi Z_2} \frac{p(r_0, t)z'}{(z'^2 + r^2 + r_0^2 - 2rr_0\cos\varphi)^{1.5}} r_0 dz' d\varphi dr_0 \\ u_r(r) &= \frac{2(1+\nu)(1-2\nu)}{\pi E} \iiint_{00Z_1}^{\infty\pi Z_2} \frac{p(r_0, t)(r - r_0\cos\varphi)}{\rho'^3(z'^2 + r^2 + r_0^2 - 2rr_0\cos\varphi)^{1.5}} r_0 dz' d\varphi dr_0 \end{aligned} \quad (1.4)$$

where: ν is the Poisson's ratio; E is the Young's modulus (GPa); $p(r_0, t)$ is the pressure change (Pa) at radial distance r_0 and time t , ϕ is the difference of azimuthal angle between surface point and the dilation center; z_1 is the depth of reservoir lower bound (m) and z_2 is the depth of reservoir upper bound (m).

Each of these solutions has been validated through numerical simulations Xu et al. (2012); Mathias et al. (2009a) or comparison with in situ observation Theis (1935). However, the analytical model used in our paper has its limitations relating to the complexity of subsurface structure and deformation processes. But the simple analytical allows us to estimate large-scale pressure change and surface displacement by considering the realistic injection and production history for hundreds of operation wells. The calculation time is fast compared to more complex models, and as we shall show, provides an adequate fit to our data.

1.5.2 Input parameters of the analytical simulations

The depth and thickness of the reservoir are irregular Han et al. (2010). In our model, we use an average thickness of 200 m, ranging from depth 2000 m to 2200 m, based on the depths of injection wells provided by Railroad Commission of Texas (RRC) and personal communication with the operator of the field. The average porosity (9.8%) and permeability (19 mD) reported by Raines (2005) were measured from a core-flooding test, which typically does not include reservoir scale imperfections such as fractures and other forms of secondary porosity. Obviously, the reservoir is very heterogeneous Han et al. (2010) but our analytical solution only requires mean porosity and permeability values. To better represent its variation, we choose three levels of porosity and permeability (low, medium and high), and predict three corresponding sets of pressure change and surface displacement. We utilize the relationship between porosity and permeability for the Canyon formation (the third sequence) given by Lucia and Kerans (2004) to calculate permeability based on three-levels of porosity (Table 1.1). Rock formation (limestone) compressibility is obtained from Newman et al. (1973). These and other properties of the reservoir formation are summarized

in Table 1.1. We further assume that the extracted hydrocarbon gas is purely methane, and that the salt concentration of injected water is 0.15 kg/l.

Fluid properties (CO_2 , water, methane and oil) at reservoir pressure (16 MPa) and temperature (41.5 °C) are summarized in Table 1.2. Properties of supercritical CO_2 and methane are obtained from the NIST fluid properties website (<http://webbook.nist.gov/chemistry/fluid/>). Properties of salt water are derived based on the empirical correlations with pressure, temperature and salt concentration shown in Mathias et al. (2009b). Density and viscosity of the produced oil are obtained from Vest Jr (1970). Oil compressibility is obtained from Satter et al. (2008).

Two geomechanical parameters, Young's modulus and Poisson's ratio, are needed for surface displacement calculation. However, there are no publicly available data for these two geomechanical properties for the overlaying Walfcamp shale. Since surface displacement is less sensitive to Poisson's ratio, a common result in many Earth deformation problems (e.g., Bevis et al., 2005), we set the value of Poisson's ratio to 0.25, and then forward model to estimate the value of Young's modulus that best fits the surface displacement observed by InSAR. We selected a profile across the significant inflation area for comparison between model simulation and InSAR observation (Figure 1). Grid search ranges are 1 – 50 GPa with search increments of 1 GPa. Goodness of fit is assessed using the standard chi-square statistic.

1.5.3 Injection and production data during 2004 - 2011

Monthly injection and production rates during 2004 to 2011 at individual wells in the field were provided by the field operator. Information concerning locations and depths of individual wells is provided by the RRC. Both CO_2 and water were injected into the reservoir from 2004 to 2011 (Figure 1.2). In detail, 409 wells injected CO_2 ; 217 wells injected water and 603 wells extracted oil and HC gas. In this field, injected CO_2 is often mixed with water, and extracted oil and HC gas are often mixed with CO_2 and water. Location of active injection and production wells during 2004 - 2011 is shown in Figure 1.5.

To reduce the computation we divide the field into grids of 500 m width (Fig. 6). We then approximate the injection/production history by placing a virtual well at the center of each grid. For CO₂ and water, we calculate the mean injection/extraction rate by adding the net fluid injection and extraction for that grid respectively. For oil and HC gas, the production rate is set equal to the net fluid extracted for that grid.

To compare with InSAR observations, we should predict surface displacement from January 2007 to March 2011. However, pressure change due to constant rate injection/production is not linear with time: fluid pressure changes significantly in the first few months and then slows down Rohmer and Raucoules (2012). Thus, for a well being operated before 2007, pressure change during 2007 to 2011 cannot be simply calculated by just using data from January 2007 to March 2011. To address this problem, we check the injection/production history of every well to see if there is any operation before 2007. If there is, we calculate pressure changes during two periods for that well: one period from the beginning of operation to March 2011 and second period from the beginning of operation to December 2006. We then subtract the pressure change during the second phase from the pressure change during the first phase to derive pressure change between January 2007 and March 2011 (the period of InSAR observations). If there is no operation prior to 2007, pressure change is calculated using data from January 2007 to March 2011. It is worth noting that fluid production and injection in the field started in 1948 and 1954 respectively, and we only have injection/production data for each well from 2004. Thus, in our simulation, the operational beginning of each well is not earlier than 2004.

1.6 Simulation results

Figure 7 shows the simulated changes in reservoir pressure due to different fluid injection/extraction rates for three assumed values of rock formation porosity and permeability. The local maxima and minima patterns are similar for the different values of porosity and permeability. Calculated pressure change in the reservoir decreases for higher values of porosity and permeability. Net CO₂ injection/production significantly affects reservoir pressure.

Since volumes of water injection and production are approximately the same (Figure 2, Figure 4b), pressure changes due to net water injection are negligible compared to those caused by net CO₂ injection, indicating that surface uplift observed by InSAR is dominated by CO₂ injection. Net water injection/production causes pressure buildup/drawdown in different areas of the field. Net oil and hydrocarbon gas production generally causes pressure drawdown in the field. In summary, pressure changes due to CO₂ injection and production are much higher than that caused by water injection/production and oil/hydrocarbon gas production.

Figure 8 shows the simulated total pressure buildup due to all fluid injection and oil/hydrocarbon gas production production for three assumed values of porosity and permeability. The low value of porosity and permeability condition yields pressure buildup up to 10 MPa, while the high value yields up to 2 MPa pressure buildup. Maximum pressure buildup is more spread out for the high porosity and permeability values.

Based on the simulated pressure change field, a grid search method was used to estimate the value of Young's modulus that best fits the InSAR observations along the profile marked in Figure 1. To compare with InSAR LOS displacement, we convert the predicted surface displacement to LOS displacement using satellite azimuth and incidence information. Figure 9 shows goodness of fit versus Young's modulus at three levels of pressure change. The best-fit values for Young's moduli are listed in Table 1.3. Predicted LOS displacements using the best-fit Young's modulus at the three levels of pressure change are compared to the InSAR data along the profile (Figure 10). All three predictions agree well with InSAR observations along the profile. The high-pressure condition provides the smallest misfit between model prediction and observation, but the difference with the other models is small. The low and medium pressure conditions also provide a good fit between model prediction and observation. However, the best-fit Young's moduli derived from the low and medium pressure conditions (6 GPa and 10 GPa) are quite small compared to the best-fit Young's modulus derived from the high-pressure condition (18 GPa), and are on the low side of plausible crustal values. A similar deformation study in south Texas Karegar et al. (2015)

where pressure data were available for calibration gave a best estimate of average Young's modulus of 55 GPa +80/-20 GPa; at 95% confidence, the minimum estimate obtained in that study was 15 GPa, similar to our high estimate. We therefore take the estimate of 18 GPa as the most plausible value for Young's modulus and the corresponding estimate of the high-pressure buildup condition (up to 10 MPa) as the best pressure change estimate.

We then predict 2D LOS displacement fields for the three models of pressure change respectively using the best-fit Young's modulus derived from the profile fitting analysis. Simulated 2D LOS displacement at the high-pressure change condition and the residual between InSAR observation and model prediction are shown in Figure 11. Our simulation is able to match most of the uplift signal observed by InSAR. However, up to 4 cm of residual uplift remains. The residuals likely reflect a combination of atmospheric and reservoir heterogeneity. The former reflects deviations from the assumption used in our data analysis that atmospheric properties are laterally uniform. The latter reflects deviations from the assumption used in our modeling that the rheological properties of the reservoir are vertically and horizontally uniform.

1.7 Discussion

We modeled a reservoir as a simplified body with uniform properties. In fact, it almost certainly has significant spatial variation in porosity, permeability and elastic properties. We have also ignored inter-well pressure interaction when simulating reservoir pressure change. Despite these simplifications, we are able to obtain good fits to the surface deformation data and obtain useful information on the reservoir. This reflects the fact that the free surface is 2000 m above the reservoir, hence the effects of reservoir heterogeneity and inter-well pressure interactions on surface deformation are relatively small. In effect, the intervening crustal material acts like a low pass filter, attenuating short wavelength strain effects associated with spatial complexities of the reservoir and the injected fluid.

The relatively large uncertainty in our estimate of Young's modulus reflects the weak resolving power of surface deformation data for this parameter. Independent determina-

tion of Young’s modulus from down-hole measurements, 3-D seismic surveys, or laboratory experiments on well bore samples would allow a more quantitative link between surface deformation and reservoir pressure change.

Gan and Frohlich (2013) suggested that increasing earthquakes in the Cogdell field, north of our study area, during 2006 – 2011 were likely triggered by CO₂ injection. However, our study area, which has also experienced significant fluid injection over the same time period, has not experienced a significant increase in seismicity. Meanwhile, InSAR data show no surface uplift in the Cogdell field, while measurable uplift is observed in our study area. The different seismic and deformation responses to fluid injection between these two fields may reflect differences in regional subsurface structures. Our study area has been mapped as a single large reef mound, but structures in the Cogdell field show more spatial variation Vest Jr (1970). The Cogdell limestone may have experienced more intense weathering and karsting compared to our study area Reid and Reid (1991), potentially creating more heterogeneous structures, and potential faults and fractures. The recent earthquakes suggest the presence of faults in the Cogdell field. The absence of mapped faults and earthquake activity in our study area suggests no active faulting. Perhaps triggered earthquakes occur when injected gas or fluid reaches suitably orientated pre-existing faults, reducing the resolved normal stress and hence the effective friction, and promoting seismic slip on pre-existing faults.

1.8 Conclusions

We evaluated injection and production data for CO₂, water, oil and hydrocarbon gas at individual wells in a CO₂-EOR field between 2004 and 2011. Approximately 50 Mt of CO₂ were sequestered between 2004 and 2011, equal to the total sequestered CO₂ between 1972 and 2003. InSAR data observe up to 10 cm line of sight displacement between January 2007 and March 2011 in this field. Water injection alone cannot explain surface uplift between January 2007 and March 2011 because net injected water (\sim 1 Mt) is negligible during this period. However, significant amounts of CO₂ (\sim 24 Mt) were injected into the reservoir,

contributing to observed surface uplift. An analytical simulation relating reservoir pressure and surface displacement using realistic injection and production data from individual wells predicts up to 10 MPa pressure buildup due to net fluid injection and production in 2007–2011, using assumed average values of porosity and permeability. With better information on the mechanical properties of the reservoir, InSAR data could directly estimate reservoir pressure changes with time.

1.9 Acknowledgements

We thank the field operator for providing historical injection and production data. We also thank the Railroad Commission of Texas for providing information on the location and depth of individual wells in our study area. This research was supported by DOE grant DE-FE0001580. We thank Karen Kluger for support and advice throughout our project and two anonymous reviewers for thoughtful comments.

1.10 References

- Berardino, P., Fornaro, G., Lanari, R., and Sansosti, E. (2002). A new algorithm for surface deformation monitoring based on small baseline differential sar interferograms. *Geoscience and Remote Sensing, IEEE Transactions on*, 40(11):2375–2383.
- Bevis, M., Alsdorf, D., Kendrick, E., Fortes, L. P., Forsberg, B., Smalley, R., and Becker, J. (2005). Seasonal fluctuations in the mass of the amazon river system and earth’s elastic response. *Geophysical research letters*, 32(16).
- Brummett Jr, W., Emanuel, A., Ronquille, J., et al. (1976). Reservoir description by simulation at sacroc-a case history. *Journal of Petroleum Technology*, 28(10):1–241.
- Bryant, S. et al. (2007). Geologic co2 storage—can the oil and gas industry help save the planet? *Journal of Petroleum Technology*, 59(09):98–105.
- Crameik, T., Plassey, J., et al. (1972). Carbon dioxide injection project sacroc unit, scurry county, texas. In *Annual Meeting Papers, Division of Production*. American Petroleum Institute.
- Dicharry, R. M., Perryman, T., Ronquille, J., et al. (1973). Evaluation and design of a co2 miscible flood project-sacroc unit, kelly-snyder field. *Journal of Petroleum Technology*, 25(11):1–309.
- Galloway, W. E., Ewing, T., Garrett, C., Tyler, N., and Bebout, D. (1983). Atlas of major texas oil reservoirs.
- Gan, W. and Frohlich, C. (2013). Gas injection may have triggered earthquakes in the cogdell oil field, texas. *Proceedings of the National Academy of Sciences*, 110(47):18786–18791.
- Han, W. S., McPherson, B. J., Lichtner, P. C., and Wang, F. P. (2010). Evaluation of trapping mechanisms in geologic co2 sequestration: Case study of sacroc northern platform, a 35-year co2 injection site. *American Journal of Science*, 310(4):282–324.

- Karegar, M. A., Dixon, T. H., Malservisi, R., Yang, Q., Hossaini, S. A., and Hovorka, S. D. (2015). Gps-based monitoring of surface deformation associated with co 2 injection at an enhanced oil recovery site. *International Journal of Greenhouse Gas Control*, 41:116–126.
- Lucia, F. J. and Kerans, C. (2004). Permeability estimation using porosity logs and rock fabric stratigraphy: an example from the sacroc (pennsylvanian) field, scurry county, texas. *PUBLICATIONS-WEST TEXAS GEOLOGICAL SOCIETY*, 4:271.
- Mathias, S. A., Hardisty, P. E., Trudell, M. R., and Zimmerman, R. W. (2009a). Approximate solutions for pressure buildup during co2 injection in brine aquifers. *Transport in Porous Media*, 79(2):265–284.
- Mathias, S. A., Hardisty, P. E., Trudell, M. R., and Zimmerman, R. W. (2009b). Screening and selection of sites for co 2 sequestration based on pressure buildup. *International Journal of Greenhouse gas control*, 3(5):577–585.
- Metz, B., Davidson, O., de Coninck, H., Loos, M., Meyer, L., et al. (2005). Carbon dioxide capture and storage.
- Morris, J. P., Hao, Y., Foxall, W., and McNab, W. (2011). A study of injection-induced mechanical deformation at the in salah co 2 storage project. *International Journal of Greenhouse Gas Control*, 5(2):270–280.
- Newman, G. et al. (1973). Pore-volume compressibility of consolidated, friable, and unconsolidated reservoir rocks under hydrostatic loading. *Journal of Petroleum Technology*, 25(02):129–134.
- Orr, F. and Taber, J. (1984). Use of carbon dioxide in enhanced oil recovery. *Science*, 224(4649):563–569.

Pepe, A. and Lanari, R. (2006). On the extension of the minimum cost flow algorithm for phase unwrapping of multitemporal differential sar interferograms. *Geoscience and Remote Sensing, IEEE Transactions on*, 44(9):2374–2383.

Raines, M. (2005). 66. kelly-snyder (cisco-canyon) fields/sacroc unit. *Oil and gas fields in west Texas*, pages 69–78.

Raines, M. and Dobitz, J. (2001). A review of the pennsylvanian sacroc unit. *PUBLICATIONS-WEST TEXAS GEOLOGICAL SOCIETY*, pages 67–74.

Reid, A. and Reid, S. T. (1991). The cogdell field study, kent and scurry counties, texas: A post-mortem. *Permian Basin Plays, Tomorrow's Technology Today: Midland, Texas, West Texas Geological Society, Publication*, pages 91–89.

Reuter, H. I., Nelson, A., and Jarvis, A. (2007). An evaluation of void-filling interpolation methods for srtm data. *International Journal of Geographical Information Science*, 21(9):983–1008.

Rinaldi, A. P. and Rutqvist, J. (2013). Modeling of deep fracture zone opening and transient ground surface uplift at kb-502 co 2 injection well, in salah, algeria. *International Journal of Greenhouse Gas Control*, 12:155–167.

Rohmer, J. and Raucoules, D. (2012). On the applicability of persistent scatterers interferometry (psi) analysis for long term co 2 storage monitoring. *Engineering Geology*, 147:137–148.

Satter, A., Iqbal, G. M., and Buchwalter, J. L. (2008). *Practical enhanced reservoir engineering: assisted with simulation software*. Pennwell Books.

Shi, J.-Q., Sinayuc, C., Durucan, S., and Korre, A. (2012). Assessment of carbon dioxide plume behaviour within the storage reservoir and the lower caprock around the kb-502 injection well at in salah. *International Journal of Greenhouse Gas Control*, 7:115–126.

Theis, C. V. (1935). *The relation between the lowering of the piezometric surface and the rate and duration of discharge of a well using ground water storage*. US Department of the Interior, Geological Survey, Water Resources Division, Ground Water Branch Washington, DC.

Vasco, D., Ferretti, A., and Novali, F. (2008). Reservoir monitoring and characterization using satellite geodetic data: Interferometric synthetic aperture radar observations from the krechba field, algeria. *Geophysics*, 73(6):WA113–WA122.

Vasco, D., Rucci, A., Ferretti, A., Novali, F., Bissell, R., Ringrose, P., Mathieson, A., and Wright, I. (2010). Satellite-based measurements of surface deformation reveal fluid flow associated with the geological storage of carbon dioxide. *Geophysical Research Letters*, 37(3).

Verdon, J. P., Kendall, J.-M., Stork, A. L., Chadwick, R. A., White, D. J., and Bissell, R. C. (2013). Comparison of geomechanical deformation induced by megatonne-scale co₂ storage at sleipner, weyburn, and in salah. *Proceedings of the National Academy of Sciences*, 110(30):E2762–E2771.

Vest Jr, E. (1970). Oil fields of pennsylvanian-permian horseshoe atoll, west texas.

White, J. A., Chiaramonte, L., Ezzedine, S., Foxall, W., Hao, Y., Ramirez, A., and McNab, W. (2014). Geomechanical behavior of the reservoir and caprock system at the in salah co₂ storage project. *Proceedings of the National Academy of Sciences*, 111(24):8747–8752.

Xu, Z., Fang, Y., Scheibe, T. D., and Bonneville, A. (2012). A fluid pressure and deformation analysis for geological sequestration of carbon dioxide. *Computers & Geosciences*, 46:31–37.

Table 1.1: Reservoir homogeneous properties used for pressure change calculation.

Reservoir Property	Symbol	Value			Unit
Porosity	φ	0.2(L)	0.25(M)	0.3(H)	%
Permeability	κ	17(L)	57(M)	152(M)	mD
Initial pressure	P_0	16			MPa
Temperature	T	41.5			°C
Depth (reservoir upper bound)	Z_1	-2000			m
Depth (reservoir lower bound)	Z_2	-2200			m
Thickness	H	200			m
Formation compressibility	C_{rock}	5.3E-10			1/Pa

Note: L, M and H represent low level, medium level and high level of porosity and permeability, respectively.

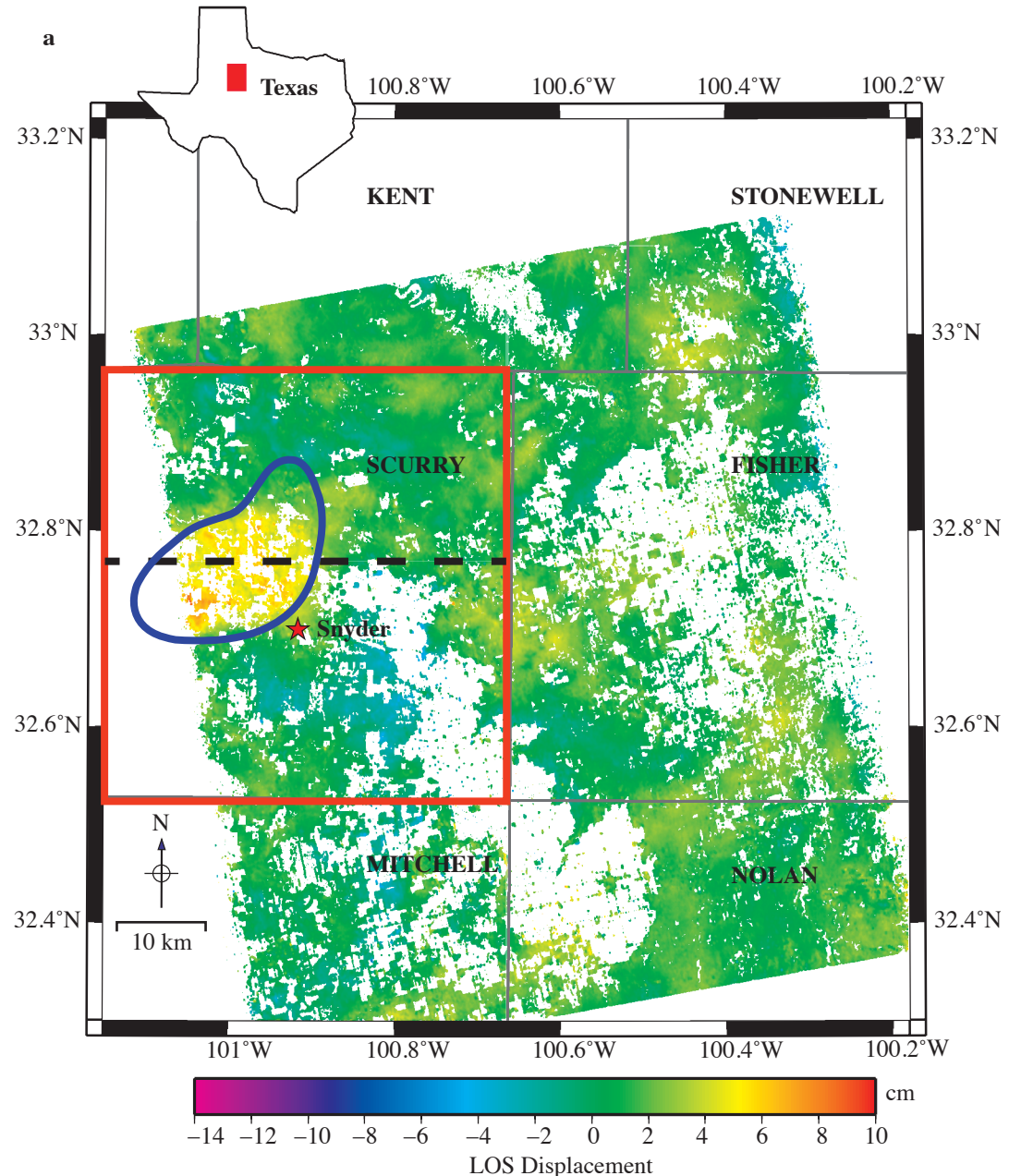
Table 1.2: Fluid properties at depth (16MPa, 41.5 °C).

Fluid property	Symbol	Value				Unit
		Brine	CO2	Methane	Oil	
Density	ρ	1105	784	115	818	kg/m ³
Viscosity	μ	9.41E-04	6.85E-05	1.67E-05	3.75E-04	Pa·s
Compressibility	C	3.40E-10	2.10E-08	5.43E-08	2.17E-09	1/Pa

Table 1.3: Highest pressure buildup and best-fit Young's modulus at three levels of porosity and permeability.

Level of porosity and permeability	Highest ΔP (MPa)	Best-fit E (GPa)	χ^2
Low	10.32	18	0.78
Medium	4.32	10	0.80
High	2.10	6	0.83

Note: E represents Young's modulus. ΔP represents calculated pressure change. χ^2 represents normalized chi square value.



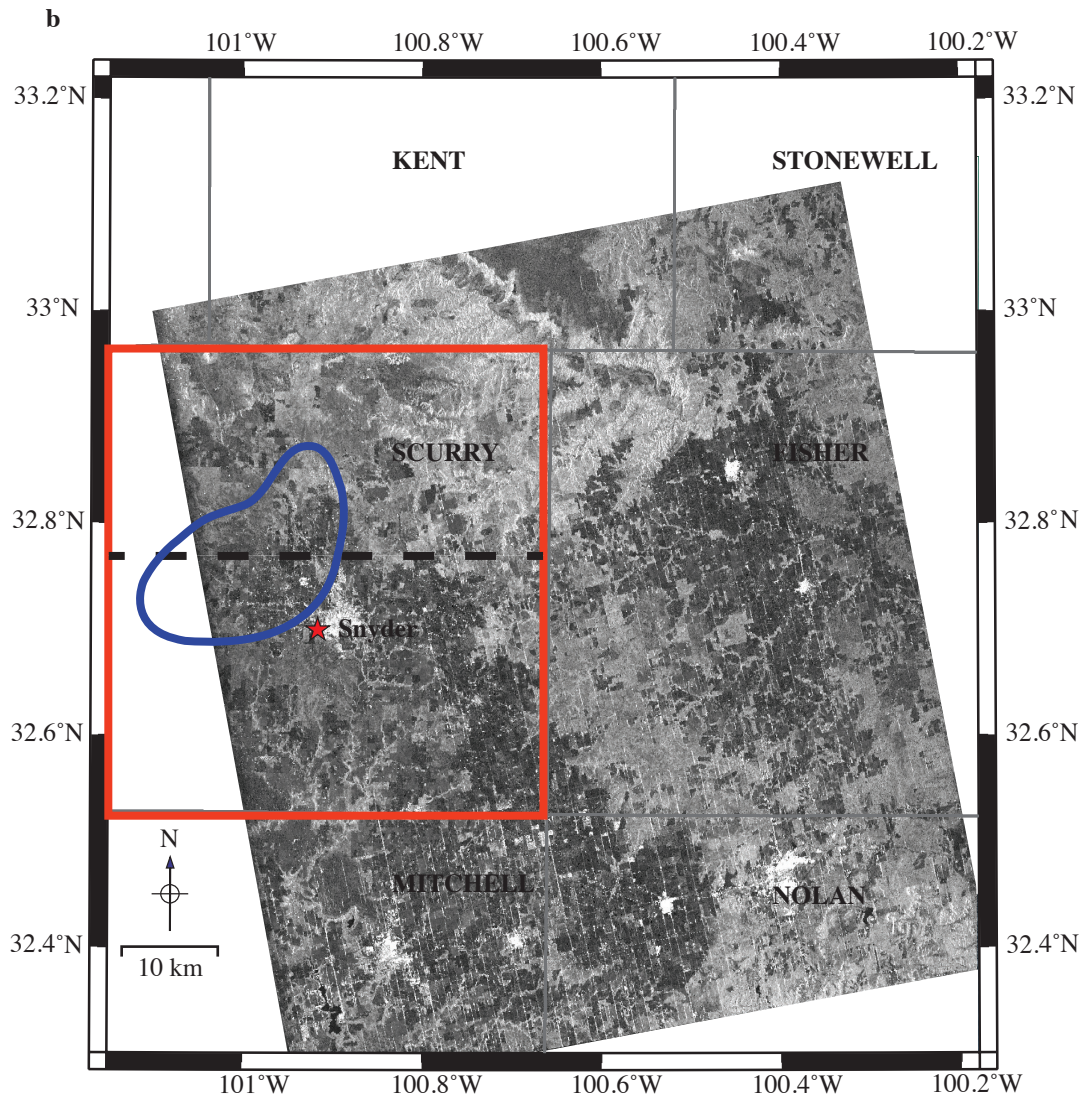


Figure 1.1: a) Total LOS (line of sight) displacement from January 08, 2007 to March 06, 2011. b) A SAR intensity image of the study area. Red star represents location of the town of Snyder, Texas. Light grey lines are county boundaries and county names are labeled. Red lines are the boundaries of our study area, Scurry County. Blue line is the approximate boundary of the oil field in the study area. Black dashed line represents location of a profile for surface displacement modeling in the following sections.

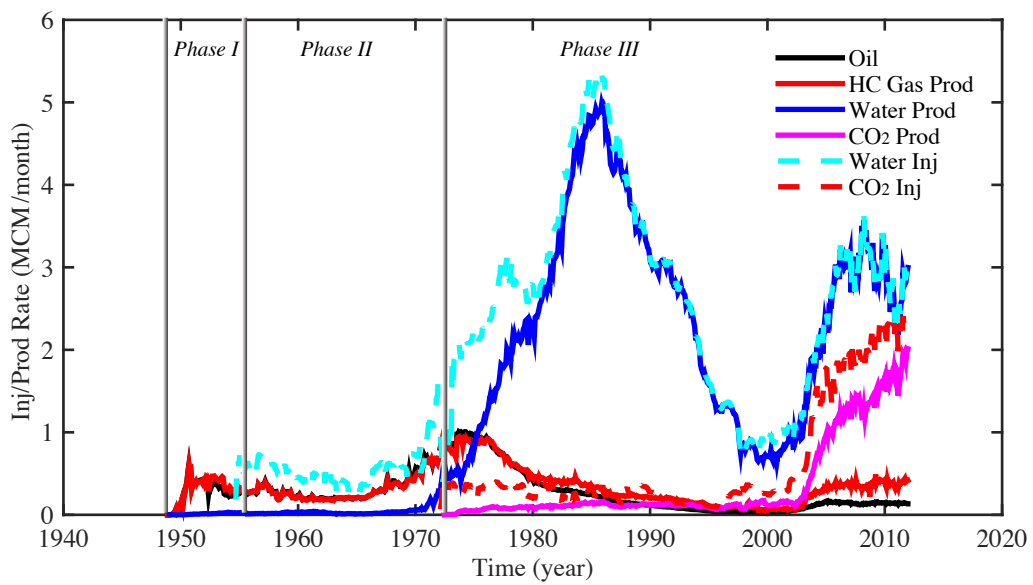


Figure 1.2: Injection and production history of the study site. Phase I is the primary recovery phase. Phase II is the secondary recovery phase. Phase III is the tertiary/enhanced oil recovery phases. Volumes of fluid injection and production are reported at 16 MPa, 41.5 °C (pressure and temperature at reservoir depth). HC is hydrocarbon.

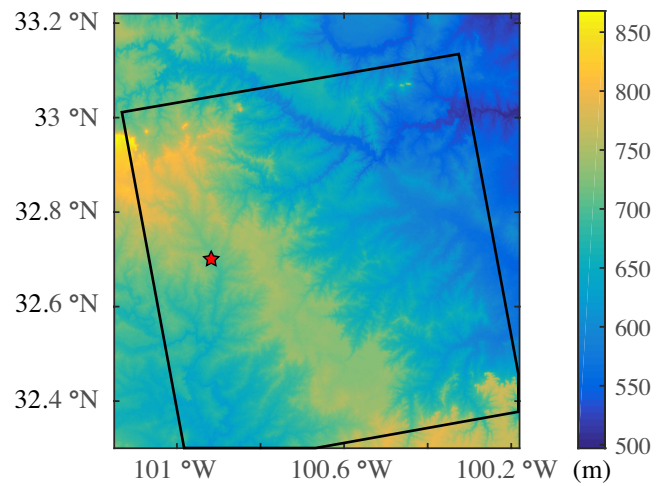


Figure 1.3: DEM of our study area. Black lines are the boundaries of the area covered by the interferogram. Red star represents location of the town Snyder, Texas.

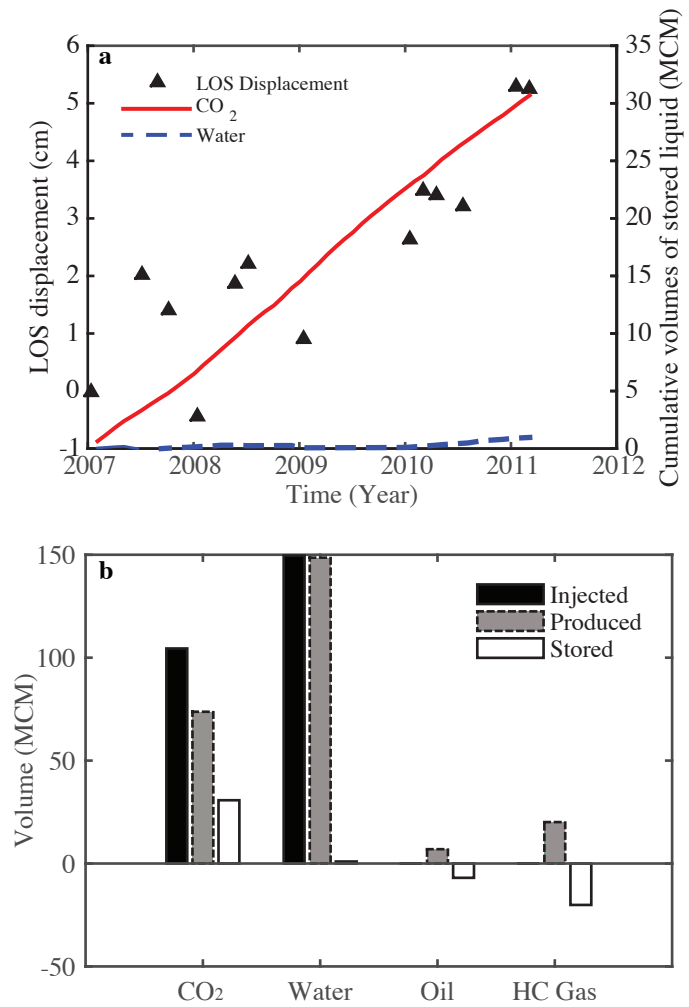


Figure 1.4: a) Comparison between Line of Sight (LOS) displacement at Snyder (red star marked in Figure 1) and cumulative volumes of stored (injection minus production) CO₂ and water in the field from January 2007 to March 2011. b) The total volumes of injected/produced/stored CO₂, water, oil and HC gas in the field from January 2007 – March 2011. Volumes of fluid injection and production are reported at 16 MPa, 41.5 °C.

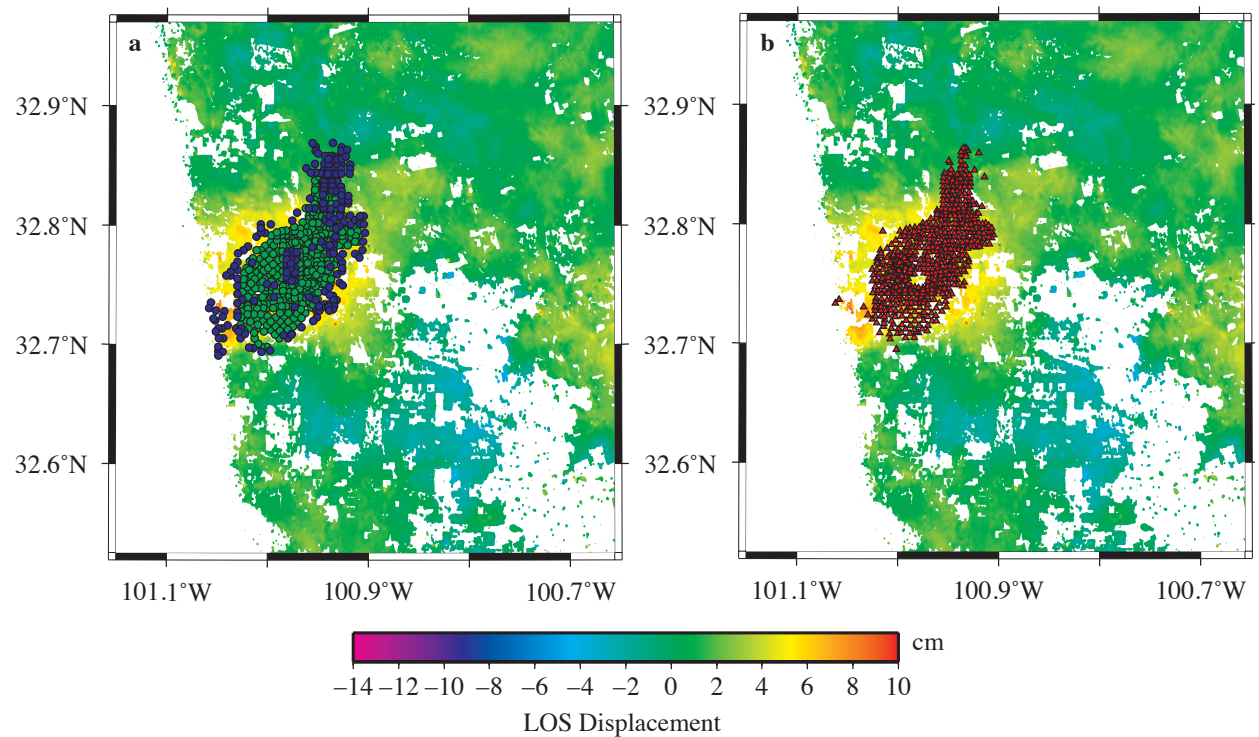


Figure 1.5: Map of study area, showing total LOS displacement from January 08, 2007 to March. 06, 2011, a) wells injecting CO₂ (green circle) and water (blue circle), and b) well producing CO₂, water, Oil and HC gas (red triangle).

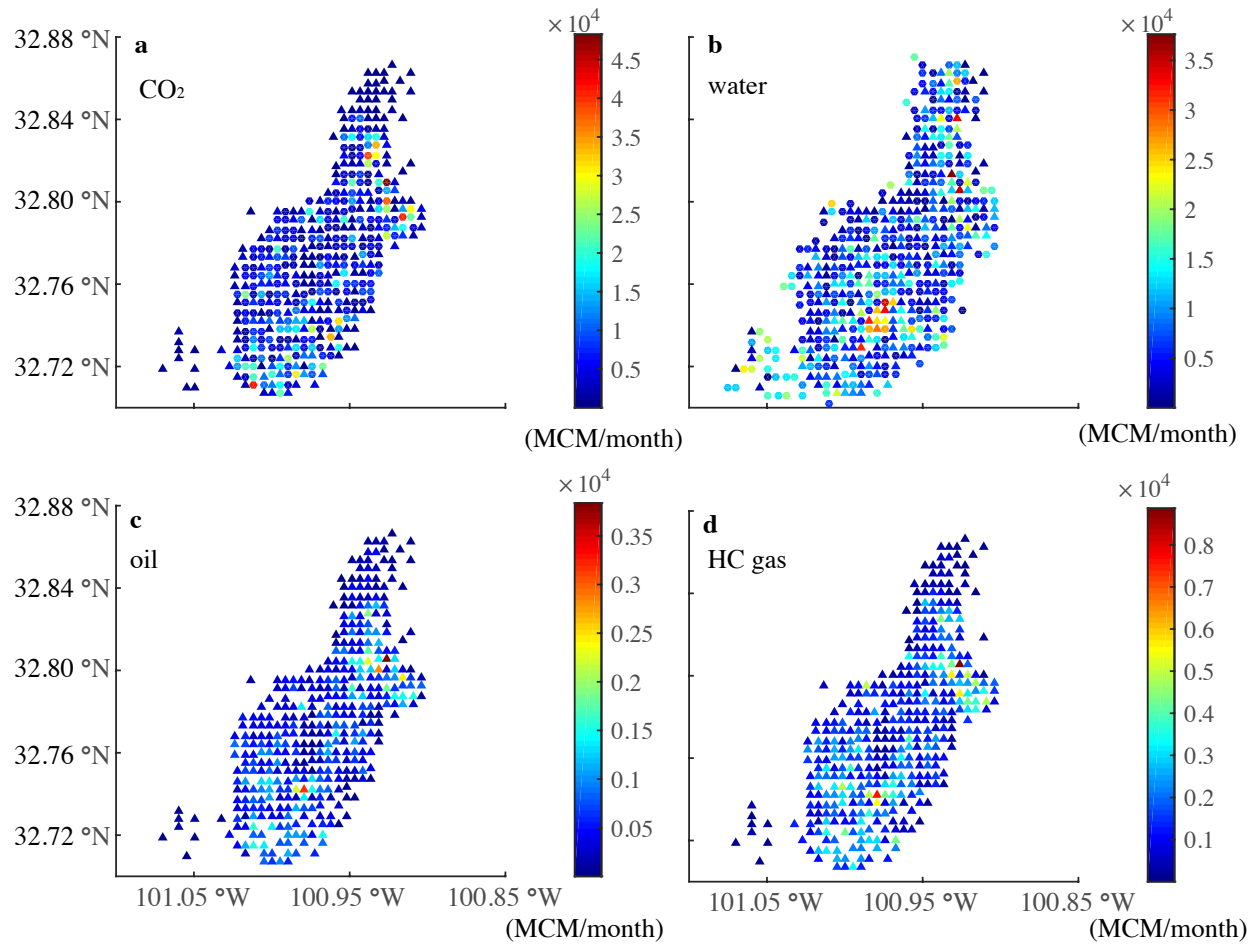


Figure 1.6: Location of virtual wells for each type fluid and the average monthly injection/production rate for each virtual well. Circles represent injection wells and triangles represent production wells. Volumes of fluid injection and production are reported at 16 MPa, 41.5 °C.

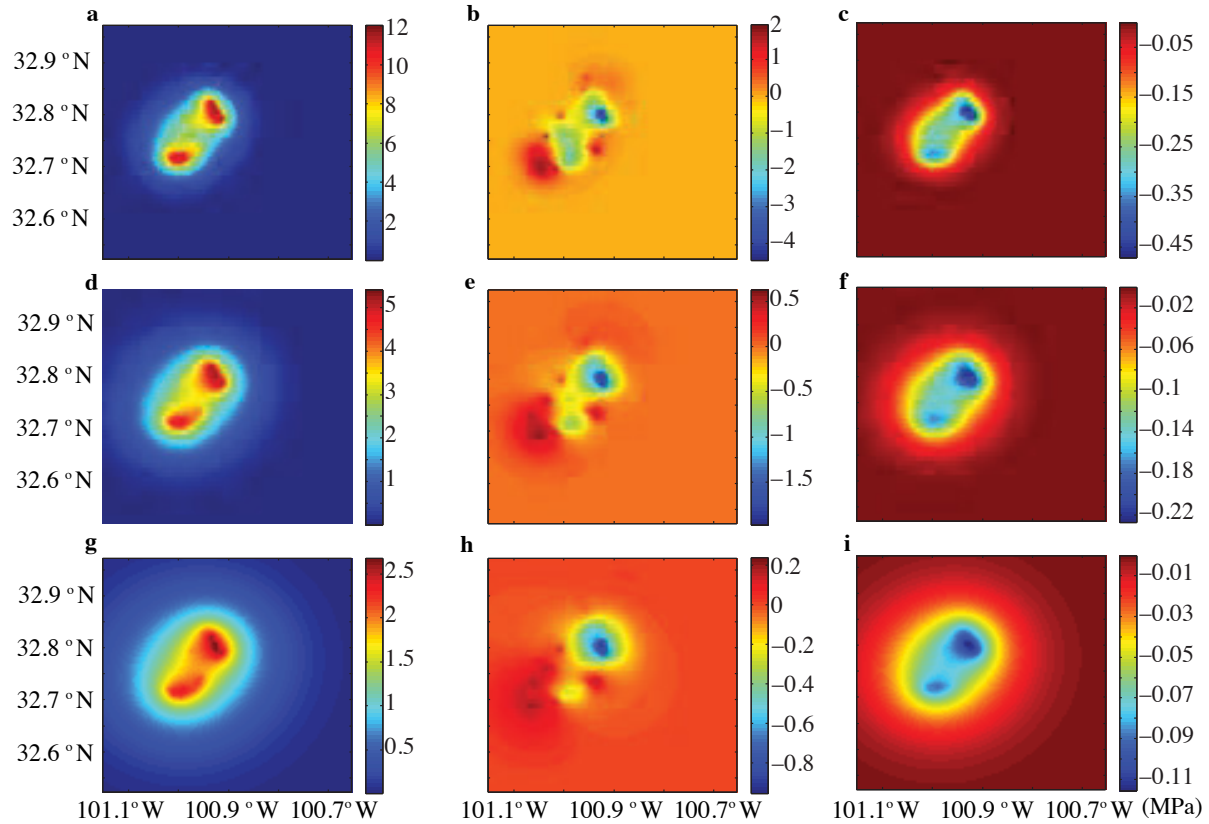


Figure 1.7: Calculated pressure change due to fluid injection and production at three levels of porosity and permeability. (a-c: low porosity/permeability; d-f: medium porosity/permeability; g-i: high porosity and permeability). a,d and g are calculated pressure buildup due to net CO_2 injection. b, e and h are derived from net water injection. c, f and I are derived from oil and HC gas production

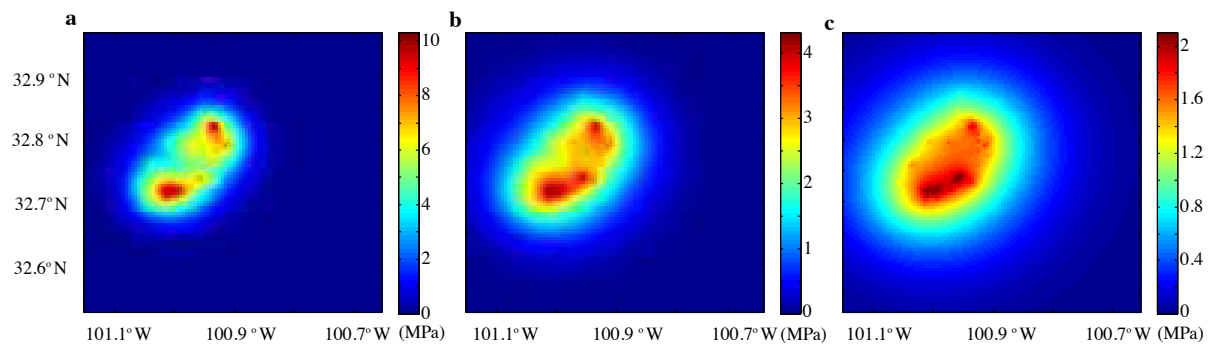


Figure 1.8: Calculated pressure change due to all injection and production activities at three levels of porosity and permeability. a) low porosity/permeability level; b) medium porosity/permeability level; c) high porosity and permeability level.

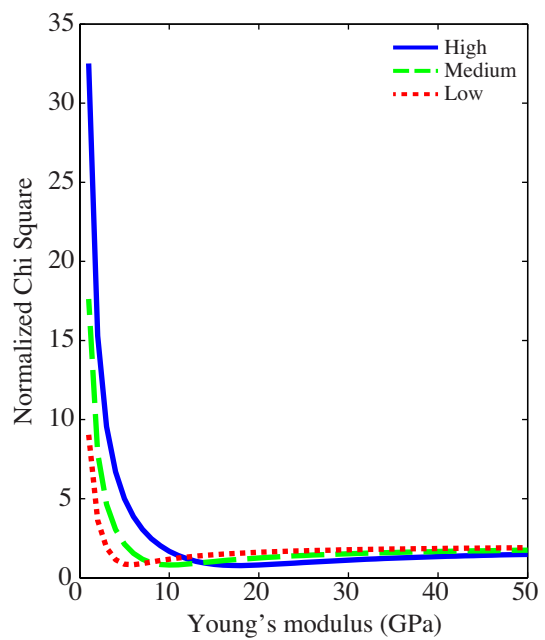


Figure 1.9: Goodness of fit versus Young's modulus at three levels of pressure change conditions. Simulated LOS displacements are fitted to LOS displacement observation along the profile shown in Figure 1. Note that the minimum value of Young's modulus is well constrained, but the upper bound value is not.

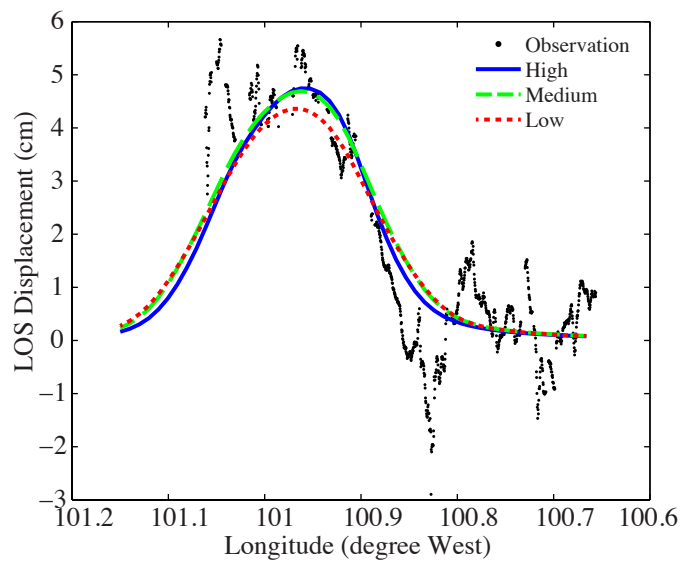


Figure 1.10: Simulated LOS displacement at three levels of pressure change conditions versus InSAR observation along the profile shown in Figure 1.

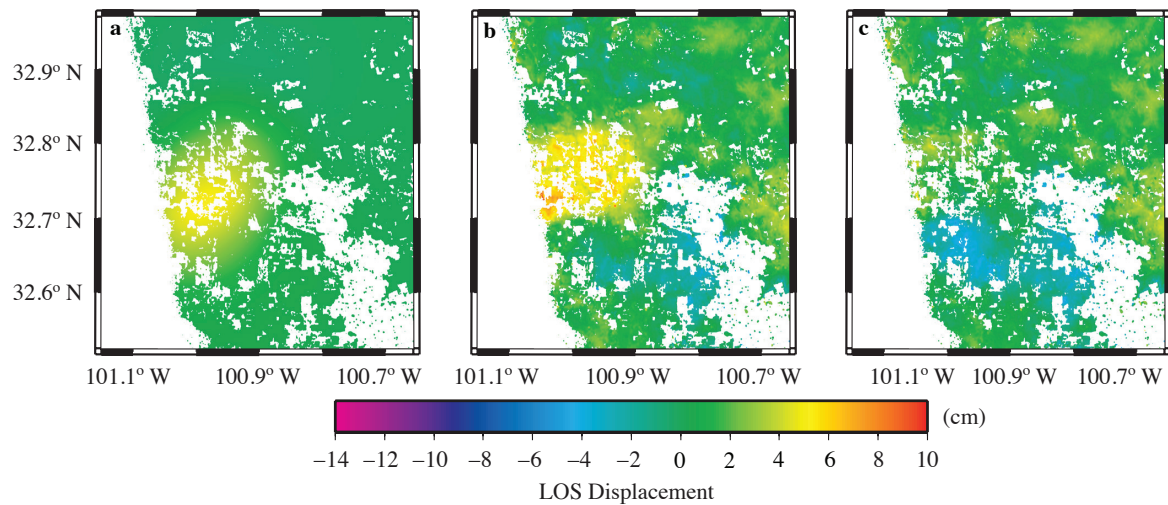


Figure 1.11: Comparison between simulated LOS displacements and InSAR observation for the entire study area. Surface displacements were derived from high-pressure change condition. a) Simulated LOS displacements; b) InSAR observation; c) residual.